THE JOURNAL OF PHYSICAL CHEMISTRY C

Article

pubs.acs.org/JPCC

Strong Thermal Transport Anisotropy and Strain Modulation in Single-Layer Phosphorene

Zhun-Yong Ong,*,† Yongqing Cai,† Gang Zhang,* and Yong-Wei Zhang

Institute of High Performance Computing, A*STAR, 138632 Singapore

ABSTRACT: Using first-principles calculations and the nonequilibrium Green's function method, we investigate ballistic thermal transport in two-dimensional monolayer phosphorene sheet. A significant crystallographic orientation dependence of thermal conductance is observed, with room temperature thermal conductance along zigzag direction being 40% higher than that along armchair direction. Furthermore, we find that the thermal conductance anisotropy with the orientation can be tuned by applying strain. In particular, the zigzag-oriented thermal conductance is enhanced when a zigzag-oriented strain is applied but decreases when an armchair-oriented strain is applied; whereas the armchair-oriented thermal conductance always decreases when either a zigzag- or an armchair-oriented strain is applied. The present work suggests that the remarkable thermal transport anisotropy and its strain-modulated effect in single-layer phosphorene may be used for thermal management in phosphorene-based electronics and optoelectronic devices.

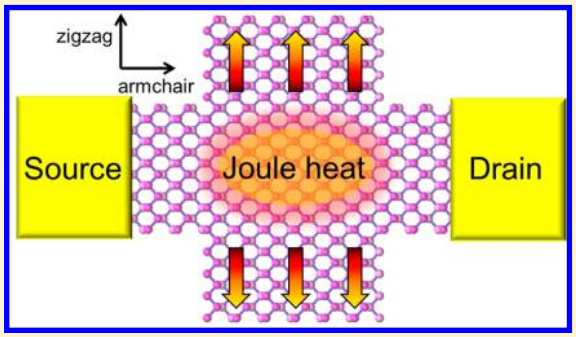

INTRODUCTION

Two-dimensional (2D) layered crystals in their single-layer form have attracted considerable attention because of the unique physical properties associated with their reduced dimensionality, which can potentially be exploited for applications in nanoscale electronic and photonic devices. For example, graphene has by far the highest carrier mobility due to its massless charge carriers,[1] while single-layer MoS_2, a member of the transition metal dichalcogenides (TMDs) family, has been regarded as a promising candidate for field effect transistor applications given its high on/off ratio.[2]

Very recently, black phosphorus (BP),[3] a layered material consisting of sheets of sp^3-hybridized phosphorus atoms puckered along the so-called in-plane armchair direction and held together by weak van der Waals forces, has been the focus of a considerable amount of research into its electronic,[4−6] optical,[7] transport,[8,9] and structural properties.[10] Part of this growing interest in BP may be attributed to the successful isolation of the few-layer forms of BP for spectroscopic and electrical characterization[9] as well as to the much larger direct band gap demonstrated in few-layer BP.[8,9] Like other ultrathin two-dimensional (2D) crystals,[11] few-layer BP also allows for superior electrostatic modulation of the carrier density, a feature that is necessary for continued nanoscale transistor scaling. Already, preliminary angle-resolved transport studies of few-layer BP show a high and significantly anisotropic hole mobility[8,12] as well as large and anisotropic in-plane optical conductivity at room temperature.[7] The single-layer form of BP, sometimes called phosphorene, is predicted to be a superior candidate material for field-effect applications given its atomic thinness and relatively high carrier mobility especially in the armchair direction.[8]

Thermal management in nanoscale electronic and optoelectronic devices remains a crucial issue,[13] especially as strong localized Joule heating in the confined volume of an ultrathin channel can reduce device reliability and performance. The use of a high thermal conductivity material in or around the transistor can help dissipate waste heat more efficiently, which is necessary for preventing device performance degradation and breakdown. Thus, the integration of a new material into a nanoscale transistor requires taking into account its thermal conduction properties. To this end, heat conduction in graphene[14−18] and in MoS_2[19−24] has been extensively studied. However, compared to these more widely studied 2D materials, the thermal transport properties of monolayer phosphorene are still not well-understood.

In this work, using the nonequilibrium Green's function (NEGF) method combined with first-principles calculations, we investigate ballistic thermal transport in a *pristine* extended monolayer sheet of phosphorene. The NEGF method yields the thermal transport behavior in the *ballistic* limit and includes the contribution of all the acoustic and optical phonon modes. In stark contrast to the isotropic thermal conductance in 2D graphene[25−27] and MoS_2 sheets, thermal transport in monolayer phosphorene exhibits strong orientation dependence. We also study how the thermal conductance varies with the magnitude and direction of the applied tensile strain. Our present study not only reveals physical insight into the thermal transport in monolayer phosphorene and but also provides a

Received: August 6, 2014
Revised: October 8, 2014
Published: October 10, 2014

dx.doi.org/10.1021/jp5079357 | J. Phys. Chem. C 2014, 118, 25272−25277

promising guideline for thermal management in phosphorene-based nanoscale devices.

METHODS

In undoped single-layer phosphorene, thermal transport is largely mediated by phonons because its relatively low electrical conductivity[9] implies that electrons only have a minor contribution to thermal transport. In a phonon-dominated system, the quantum thermal conductance can be calculated using the standard nonequilibrium Green's function (NEGF) method.[28] According to the well-known Landauer theory, the phonon-derived thermal conductance can be expressed as[28]

$$G(T) = \frac{1}{2\pi S}\int_0^\infty d\omega\hbar\omega\frac{df}{dT}\Xi(\omega) \quad (1)$$

where S is the cross-sectional area with the strain in the transverse direction being taken into account and f is the Bose–Einstein distribution function. The thickness of the phosphorene layer is assumed to be 0.55 nm. The transmittance or transmission function $\Xi(\omega)$ is calculated using the more general plane-wave formulation of the NEGF method described in ref 29, which essentially computes the ballistic thermal current for an infinitely wide and extended sample by averaging over the phonon transmission associated with each transverse wave vector ($k_\parallel$) because the phosphorene sheet is infinitely large and translationally invariant in the direction transverse and parallel to the heat current (unlike the case for nanoribbons). As some of the optical phonon branches have considerably high group velocity, their contribution to thermal conduction cannot be neglected.[30] The plane-wave formulation of the NEGF method[29] enables us to compute the ballistic contribution from all acoustic and optical phonon modes. A detailed derivation and description of the NEGF method, as applied to systems translationally invariant in the direction perpendicular to the heat current, can be found in ref 29.

In this work, the interatomic force constants for all the phosphorus structures are calculated from first-principles calculation based on density functional theory (DFT) by using the QUANTUM ESPRESSO package.[31] We employ the local density functional together with the Trouiller–Martins-type[32] norm-conserving pseudopotentials. A cutoff energy of 50 Ry for the plane waves and a 14 × 10 × 1 Monkhorst–Pack k-point are adopted. Each phosphorus slab is separated by a vacuum of 15 Å normal to the surface. The atomic coordinates and the lattice constants are relaxed until the forces exerted on the atoms are less than 0.01 eV/Å and the stress less than 0.01 kbar. At zero strain, the lattice constants are a_1 = 3.263 Å and a_2 = 4.341 Å. The dynamical matrix based on an 8 × 6 × 1 grid of q points is calculated by using the density functional perturbation theory (DFPT), and the real space force constants are then obtained by the inverse Fourier transform of the dynamical matrix at each q grid.

RESULTS AND DISCUSSION

Phonon Dispersion. Structurally, bulk BP is a layered material similar to graphite but with each layer consisting of an undulating array of ridges parallel to the zigzag direction, resembling an accordion.[33] Hence, its mechanical properties are highly anisotropic. The elastic stiffness constants and sound velocities have been measured to be much larger along the zigzag direction than along the armchair direction in bulk BP.[33,34] The linear compressibility is also much higher in the armchair direction than in the zigzag direction.[35] Likewise, we expect the phonon properties of single-layer phosphorene to be similarly orientation-dependent.

Figure 1 shows the phonon dispersion in the Γ–X (zigzag) and Γ–Y (armchair) directions. Around the Γ-point, the

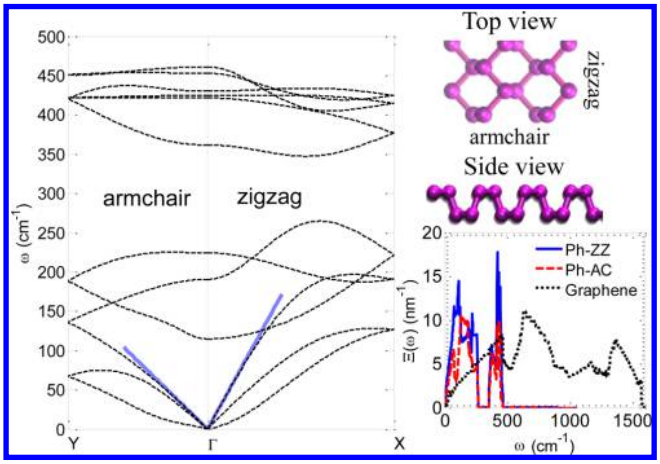

Figure 1. Phonon dispersion along the Γ–X (zigzag) and Γ–Y (armchair) directions in single-layer phosphorene. The longitudinal acoustic phonon velocity is higher in the zigzag direction. The side view shows the accordion-like structure along the armchair direction. The bottom right compares the phonon transmission spectrum for phosphorene in the zigzag (Ph–ZZ) and armchair (Ph–AC) directions with that for graphene.

longitudinal acoustic (LA) phonon velocity is significantly higher in the zigzag direction because of the greater stiffness in the zigzag direction, as suggested by the accordion-like structure. This difference in the phonon velocities implies that there would be significant orientation dependence in the thermal transport, with the thermal conductance in the zigzag direction being greater.

Since monolayer phosphorene contains 4 atoms in the unit cell, there are total of 12 modes of vibration. On the basis of the orthorhombic symmetry, the irreducible representations of the 9 optical modes at the Γ point are $B_{1u} + B_{2u} + B_{2g} + 2B_{3g} + 2A_g + A_u + B_{1g}$. All the even parity modes are Raman active, whereas the odd B_{1u} and B_{2u} modes are IR active. For bulk BP, its unit cell also contains four phosphorus atoms although the unit cell atoms are equally distributed over two adjacent monolayers. Bulk BP has the same number and symmetry classification of modes as monolayer BP, owing to the puckered structure.

We also compare the phonon transmittance spectrum of monolayer phosphorene in the zigzag and armchair directions with that of monolayer graphene as shown in Figure 1. Unlike graphene, the phonon transmission in phosphorene primarily comprises sub-500 cm^{-1} modes, while the phonon transmittance in graphene includes more higher-frequency (>500 cm^{-1}) modes.

Anisotropic Thermal Conductance under Biaxial Strain. Figure 2a shows the thermal conductance in the zigzag (G_{zigzag}) and armchair ($G_{armchair}$) directions at different biaxial tensile strain values (0, 2, and 4%) as a function of temperature from T = 10 to 1000 K. At room temperature (T = 300 K), G_{zigzag} and $G_{armchair}$ for phosphorene with 0% strain are equal to 1.08 and 0.76 nW/K/nm^2, respectively. The value for G_{zigzag} is comparable to that for MoS_2 (~1.28 nW/K/nm^2)[36] but much lower than that for graphene (~4.1 nW/K/nm^2).[37] This low

dx.doi.org/10.1021/jp5079357 | J. Phys. Chem. C 2014, 118, 25272–25277

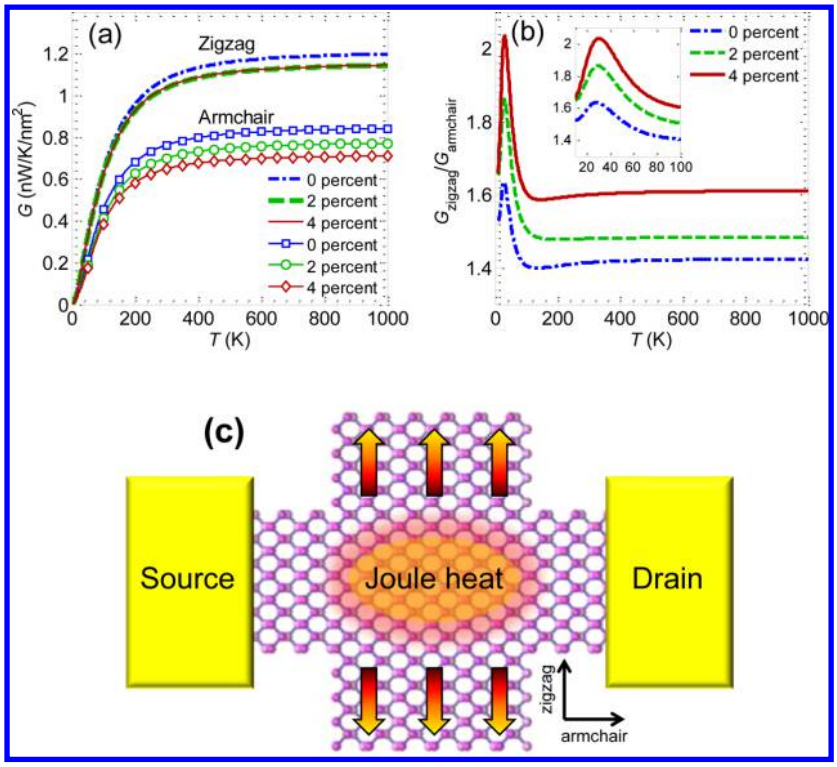

Figure 2. (a) Plot of the thermal conductance in the zigzag (G_{zigzag}) and armchair ($G_{armchair}$) directions as a function of temperature at different strain values (0, 2, and 4%) for biaxial strain. (b) Plot of their ratio ($G_{zigzag}/G_{armchair}$) as a function of temperature. The inset shows the ratio at low temperature. (c) Schematic of the cross-shape device structure for dissipating heat away in the direction transverse to the electrical current.

thermal conductance may be due to the nonplanar structure of the single-layer phosphorene. More interestingly, in stark contrast to the isotropic thermal conductance observed in monolayer graphene and MoS_2 sheets,[19−21] monolayer phosphorene exhibits a significant anisotropy in its thermal conductance. Figure 2b shows the thermal conductance ratio $G_{zigzag}/G_{armchair}$ as a function of temperature. At room temperature, G_{zigzag} is about 40% larger than $G_{armchair}$, i.e., $G_{zigzag}/G_{armchair} \approx 1.4$. The anisotropy ratio increases as the temperature decreases, attaining a peak value of 1.6 at around 28 K at zero strain.

This anisotropy in thermal conduction has implications for heat dissipation in 2D crystal-based nanoscale devices where Joule heating in the confined volume of the atomically thin crystal can create localized hot spots[38−40] and the management of waste heat is expected to be a design bottleneck to the large-scale transistor integration into functional circuit. In graphene, which has a high thermal conductivity (~2000 to 5000 W/K/m), Joule heat is expected to diffuse toward the metal electrodes, which act as heat sinks.[38,40] However, in monolayer phosphorene, the carrier mobility is considerably higher along the armchair direction than along the zigzag direction. Thus, in a phosphorene field effect transistor, the source-drain electrical current should be aligned in the armchair direction, which is unfortunately also the direction with the inferior thermal conductance, around 20% of that of graphene. Thus, new design strategies for the thermal management of phosphorene-based electrical and optoelectronic devices are needed. The relatively higher thermal conductance along the zigzag direction suggests that heat dissipation should be channeled transversely rather than to metal source/drain electrodes. The cross-shape device structure shown in Figure 2c allows the electrical current to flow along armchair direction while enabling heat to be dissipated transversely, taking advantage of the superior thermal conductance in the zigzag direction.

Next, we explore the effect of biaxial strain on the thermal conductance of monolayer phosphorene. Figure 2a shows both G_{zigzag} and $G_{armchair}$ decreasing as a function of strain (0 to 4%). The thermal conductance reduction with increasing tensile strain is consistent with that observed in graphene[41−43] and other nanostructures.[44] However, the decrease is proportionally larger for $G_{armchair}$ than for G_{zigzag}. In the zigzag direction, the change is much smaller with the conductance change between 2 and 4% strain being almost imperceptible. Figure 2b shows the thermal conductance ratio $G_{zigzag}/G_{armchair}$ as a function of temperature. At 300 K, the $G_{zigzag}/G_{armchair} \approx 1.4$ for zero strain. However, as the strain increases to 4%, the ratio rises to 1.6 because $G_{armchair}$ decreases by a larger relative extent. This indicates that the conductance anisotropy can be enhanced by applying a biaxial strain. We also observe that at low temperatures (T < 100 K), the anisotropy peaks at around 28 K with a value of 1.6 for zero strain, rising to 2.0 at 4% strain.

Anomalous Effects under Uniaxial Strain. The change in thermal conductance under biaxial strain shows that the strain affects $G_{armchair}$ more than G_{zigzag}. To understand the mechanism more deeply, we apply a uniaxial strain in each direction and observe the change in thermal conductance. Figure 3 shows the thermal conductance in the zigzag (G_{zigzag}) and armchair ($G_{armchair}$) directions as a function of temperature (T = 10 to 1000 K) for strain applied in the (a) zigzag and (b) armchair direction. $G_{armchair}$ decreases as we increase the strain in either the armchair or the zigzag direction. As expected, the decrease for uniaxial strain is not as great as the decrease for biaxial strain where we apply strain along both directions simultaneously. This also shows that the change in $G_{armchair}$ is

dx.doi.org/10.1021/jp5079357 | J. Phys. Chem. C 2014, 118, 25272−25277

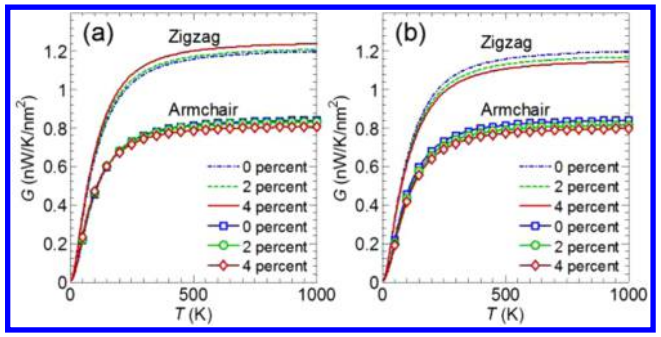

Figure 3. Plot of the thermal conductance in the zigzag (G_{zigzag}) and armchair ($G_{armchair}$) direction as a function of temperature at different strain values (0, 2, and 4%) for uniaxial strain applied in the (a) zigzag and (b) armchair directions.

relatively insensitive to the direction of the applied strain. The decrease in $G_{armchair}$ under tensile strain is similar to the trend observed in thermal transport simulations of bulk silicon and diamond, which has been explained as originating from the lower phonon group velocities when strain is applied.[44]

However, we find that G_{zigzag} exhibits an anomalous orientation-dependent change. When the strain is applied in the armchair direction, G_{zigzag} decreases like $G_{armchair}$. However, when the tensile strain is applied in the zigzag direction, G_{zigzag} actually *increases* by a small but perceptible amount. This anomaly in the change in G_{zigzag} and $G_{armchair}$ implies that the thermal conductance anisotropy can be modulated by changing the direction of the applied strain. Figure 4 shows the

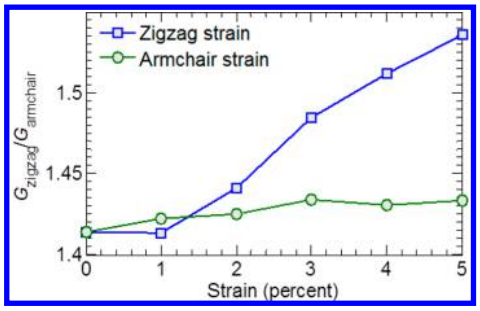

Figure 4. Plot of the thermal conductance anisotropy ($G_{zigzag}/G_{armchair}$) at different strain values (0 to 5%) for uniaxial strain applied in the zigzag (square) and armchair (circle) directions at 300 K.

anisotropy ratio ($G_{zigzag}/G_{armchair}$) as a function of the applied strain (0 to 5%) in the zigzag and armchair directions. The anisotropy ratio is ~1.4 for zero strain, but as we increase the strain, the ratio rises. This rise in the anisotropy ratio is substantially greater for strain in the zigzag direction than in the armchair direction.

Transmittance Analysis. To understand the nontrivial strain effects on thermal conductance, we plot the phonon transmittance along the zigzag direction ($\Xi_{zigzag}(\omega)$, Figure 5a) and armchair direction ($\Xi_{armchair}(\omega)$, Figure 5b), respectively, for strain applied in the zigzag direction. In the plot of the transmittances, the spectrum gives the frequency-dependent relative contribution to the thermal conductance. We find that the strain in the zigzag direction results in markedly phonon softening, which we observe from the red-shift in the high-energy ($\omega > 350$ cm^{-1}) optical phonon transmittance. Another consequence of the strain is that the low frequency ($\omega < 120$ cm^{-1}) Ξ_{zigzag} is enhanced. In contrast, when the strain is applied

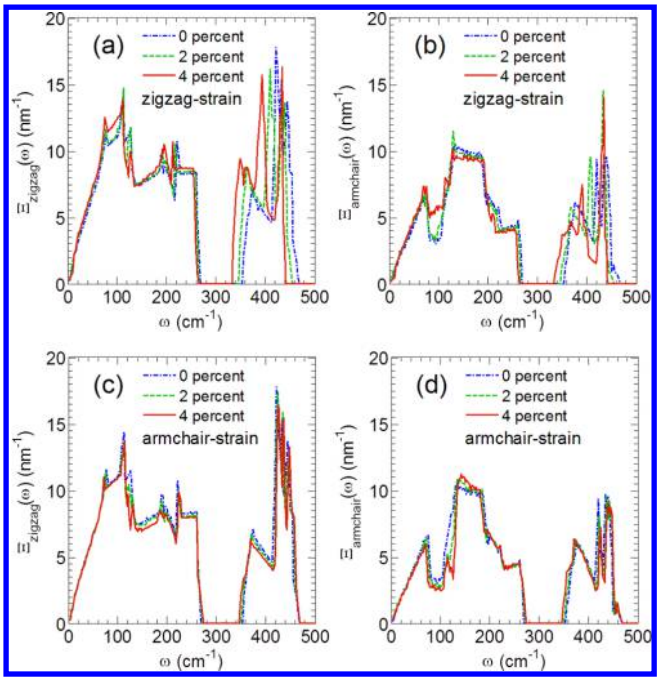

Figure 5. Plot of the zigzag and armchair-oriented cross-sectional phonon transmission (Ξ_{zigzag} and $\Xi_{armchair}$) as a function of frequency at different strain values (0, 2, and 4%) for uniaxial strain applied in the (a,b) zigzag and (c,d) armchair directions.

in the armchair direction, the frequency redshift in $\Xi_{zigzag}(\omega)$ (Figure 5c) and $\Xi_{armchair}(\omega)$ (Figure 5d) are much smaller. There is also a small but visible reduction in the phonon transmittances, which explains the decrease in G_{zigzag} and $G_{armchair}$ in Figure 3b.

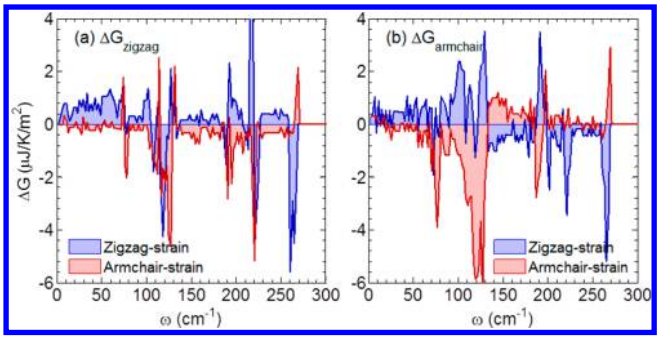

Figure 6. Plot of the differential thermal conductance ΔG for thermal transport in the (a) zigzag and (b) armchair directions, under tensile strain.

To understand how strain affects the relative contribution from phonons at different frequencies, we plot in Figure 6 the differential thermal conductance, which is defined as

$$\Delta G(\omega) = \frac{\hbar\omega}{2\pi S}\frac{df}{dT}\Delta\Xi(\omega) \quad (2)$$

where $\Delta\Xi$ is the difference in the transmittance at 2 and 0% strain, for thermal transport in the (a) zigzag and (b) armchair directions. We set the temperature to be 300 K. $\Delta G(\omega)$ measures the *contribution* to the change in total thermal conductance by phonon modes with frequency ω, with respect

dx.doi.org/10.1021/jp5079357 | J. Phys. Chem. C 2014, 118, 25272−25277

to the 2% tensile strain (zigzag or armchair). A large $\Delta G(\omega)$ corresponds to a significant contribution to the change in thermal conductance by phonons with frequency ω.

It is interesting to find that with uniaxial strain along either the armchair or zigzag direction, the contribution by the high-frequency (ω > 350 cm^{-1}) optical phonons to ΔG_{zigzag} and $\Delta G_{armchair}$ is negligible. With strain in the armchair direction, most of the change in the thermal conductance (ΔG_{zigzag} and $\Delta G_{armchair}$) is due to the drop in the low-frequency acoustic phonon contribution (60 to 260 cm^{-1} for ΔG_{zigzag} and 60 to 140 cm^{-1} for $\Delta G_{armchair}$). Thus, the reduced acoustic phonon transmittance is responsible for the decrease in the thermal conductance (both $G_{armchair}$ and G_{zigzag}) with strain in the armchair direction. However, when tensile strain is applied in the zigzag direction, there is an increase in the acoustic and optical phonon contribution between 0 and 260 cm^{-1} to G_{zigzag}. The opposite trend is observed for $G_{armchair}$: there is a corresponding drop in the acoustic and optical phonon contribution over the same frequency range. Thus, with strain along zigzag direction, G_{zigzag} increases with strain, while $G_{armchair}$ changes only slightly.

Although the scope of our work is limited to ballistic thermal conduction in perfect monolayer phosphorene, it is worth mentioning that most materials have natural point defects, such as isotopes, vacancies, and other crystallographic defects. Recently, the effect of point defects on the electronic properties of monolayer phosphorene was investigated. It was found that intrinsic point defects are electronically inactive in monolayer phosphorene, which are quite different from those in heteroelemental system.[45] For thermal conduction, in general, since the phonon frequency depends on mass, such point defects can lead to increased phonon scattering, which introduces localized vibrational modes and reduces thermal conductivity.[46] The effect of point defect on thermal conductance of monolayer phosphorene is a promising line for future investigation.

Summary. We have found a strong anisotropy in thermal conductance of single-layer phosphorene: thermal conductance is much larger in the zigzag direction than in the armchair direction. Under the application of tensile strain in the armchair direction, the thermal conductance in the armchair and zigzag directions ($G_{armchair}$ and G_{zigzag}) decreases as expected. However, when the strain is in the zigzag direction, the $G_{armchair}$ decreases while G_{zigzag} increases. This anomalous strain dependence in G_{zigzag} can be attributed to the increase in enhanced contribution of the low-frequency phonon modes when the strain is applied in the zigzag direction. By combining the reported high carrier mobility along the armchair direction and the observed high thermal conductance along the zigzag direction in the present work, a cross-shape device structure is suggested for the thermal management of phosphorene-based electrical and optoelectronic devices. Moreover, our results also suggest that thermal transport in single-layer phosphorene can be modulated via applying tensile strain.

AUTHOR INFORMATION

Corresponding Authors

*(Z.-Y.O.) E-mail: ongzy@ihpc.a-star.edu.sg;.
*(G.Z.) E-mail: zhangg@ihpc.a-star.edu.sg.

Author Contributions

†These authors contributed equally to this work.

Notes

The authors declare no competing financial interest.

ACKNOWLEDGMENTS

We acknowledge the funding support from the Agency for Science, Technology and Research, Singapore.

REFERENCES

(1) Castro Neto, A. H.; Guinea, F.; Peres, N. M. R.; Novoselov, K. S.; Geim, A. K. The Electronic Properties of Graphene. *Rev. Mod. Phys.* **2009**, *81* (1), 109−162.

(2) Butler, S. Z.; Hollen, S. M.; Cao, L.; Cui, Y.; Gupta, J. A.; Gutiérrez, H. R.; Heinz, T. F.; Hong, S. S.; Huang, J.; Ismach, A. F.; et al. Progress, Challenges, and Opportunities in Two-Dimensional Materials Beyond Graphene. *ACS Nano* **2013**, *7* (4), 2898−2926.

(3) Morita, A. Semiconducting Black Phosphorus. *Appl. Phys. A: Mater. Sci. Process.* **1986**, *39* (4), 227−242.

(4) Rodin, A. S.; Carvalho, A.; Castro Neto, A. H. Strain-Induced Gap Modification in Black Phosphorus. *Phys. Rev. Lett.* **2014**, *112* (17), 176801.

(5) Rudenko, A. N.; Katsnelson, M. I. Quasiparticle Band Structure and Tight-Binding Model for Single- and Bilayer Black Phosphorus. *Phys. Rev. B* **2014**, *89* (20), 201408.

(6) Zhu, Z.; Tománek, D. Semiconducting Layered Blue Phosphorus: A Computational Study. *Phys. Rev. Lett.* **2014**, *112* (17), 176802.

(7) Buscema, M.; Groenendijk, D. J.; Blanter, S. I.; Steele, G. A.; van der Zant, H. S. J.; Castellanos-Gomez, A. Fast and Broadband Photoresponse of Few-Layer Black Phosphorus Field-Effect Transistors. *Nano Lett.* **2014**, *14* (6), 3347−3352.

(8) Li, L.; Yu, Y.; Ye, G. J.; Ge, Q.; Ou, X.; Wu, H.; Feng, D.; Chen, X. H.; Zhang, Y. Black Phosphorus Field-Effect Transistors. *Nat. Nano* **2014**, *9* (5), 372−377.

(9) Liu, H.; Neal, A. T.; Zhu, Z.; Luo, Z.; Xu, X.; Tománek, D.; Ye, P. D. Phosphorene: An Unexplored 2d Semiconductor with a High Hole Mobility. *ACS Nano* **2014**, *8* (4), 4033−4041.

(10) Fei, R.; Yang, L. Strain-Engineering the Anisotropic Electrical Conductance of Few-Layer Black Phosphorus. *Nano Lett.* **2014**, *14*, 2884−2889.

(11) Jariwala, D.; Sangwan, V. K.; Lauhon, L. J.; Marks, T. J.; Hersam, M. C. Emerging Device Applications for Semiconducting Two-Dimensional Transition Metal Dichalcogenides. *ACS Nano* **2014**, *8* (2), 1102−1120.

(12) Xia, F.; Wang, H.; Jia, Y. Rediscovering Black Phosphorus as an Anisotropic Layered Material for Optoelectronics and Electronics. *Nat. Commun.* **2014**, *5*, 4458.

(13) Pop, E. Energy Dissipation and Transport in Nanoscale Devices. *Nano Res.* **2010**, *3* (3), 147−169.

(14) Balandin, A. A. Thermal Properties of Graphene and Nanostructured Carbon Materials. *Nat. Mater.* **2011**, *10* (8), 569−581.

(15) Sadeghi, M. M.; Pettes, M. T.; Shi, L. Thermal Transport in Graphene. *Solid State Commun.* **2012**, *152* (15), 1321−1330.

(16) Pop, E.; Varshney, V.; Roy, A. K. Thermal Properties of Graphene: Fundamentals and Applications. *MRS Bull.* **2012**, *37* (12), 1273−1281.

(17) Yang, N.; Xu, X.; Zhang, G.; Li, B. Thermal Transport in Nanostructures. *AIP Adv.* **2012**, *2* (4), 041410.

(18) Shahil, K. M. F.; Balandin, A. A. Thermal Properties of Graphene and Multilayer Graphene: Applications in Thermal Interface Materials. *Solid State Commun.* **2012**, *152* (15), 1331−1340.

(19) Liu, X.; Zhang, G.; Pei, Q.-X.; Zhang, Y.-W. Phonon Thermal Conductivity of Monolayer MoS_2 Sheet and Nanoribbons. *Appl. Phys. Lett.* **2013**, *103* (13), 133113.

(20) Li, W.; Carrete, J.; Mingo, N. Thermal Conductivity and Phonon Linewidths of Monolayer MoS_2 from First Principles. *Appl. Phys. Lett.* **2013**, *103* (25), 253103.

(21) Sahoo, S.; Gaur, A. P. S.; Ahmadi, M.; Guinel, M. J. F.; Katiyar, R. S. Temperature-Dependent Raman Studies and Thermal Con-

ductivity of Few-Layer MoS_2. *J. Phys. Chem. C* **2013**, *117* (17), 9042−9047.
(22) Jiang, J.-W.; Park, H. S.; Rabczuk, T. Molecular Dynamics Simulations of Single-Layer Molybdenum Disulphide (MoS_2): Stillinger-Weber Parametrization, Mechanical Properties, and Thermal Conductivity. *J. Appl. Phys.* **2013**, *114* (6), 064307.
(23) Yan, R.; Simpson, J. R.; Bertolazzi, S.; Brivio, J.; Watson, M.; Wu, X.; Kis, A.; Luo, T.; Hight Walker, A. R.; Xing, H. G. Thermal Conductivity of Monolayer Molybdenum Disulfide Obtained from Temperature-Dependent Raman Spectroscopy. *ACS Nano* **2013**, *8* (1), 986−993.
(24) Wei, X.; Wang, Y.; Shen, Y.; Xie, G.; Xiao, H.; Zhong, J.; Zhang, G. Phonon Thermal Conductivity of Monolayer MoS_2: a Comparison with Single Layer Graphene. *Appl. Phys. Lett.* **2014**, *105* (10), 103902.
(25) Nika, D. L.; Askerov, A. S.; Balandin, A. A. Anomalous Size Dependence of the Thermal Conductivity of Graphene Ribbons. *Nano Lett.* **2012**, *12* (6), 3238−3244.
(26) Cocemasov, A. I.; Nika, D. L.; Balandin, A. A. Phonons in Twisted Bilayer Graphene. *Phys. Rev. B* **2013**, *88* (3), 035428.
(27) Denis, L. N.; Balandin, A. A. Two-Dimensional Phonon Transport in Graphene. *J. Phys.: Condens. Matter* **2012**, *24* (23), 233203.
(28) Zhang, W.; Fisher, T. S.; Mingo, N. The Atomistic Green's Function Method: An Efficient Simulation Approach for Nanoscale Phonon Transport. *Numer. Heat Transfer, Part B* **2007**, *51* (4), 333−349.
(29) Zhang, W.; Fisher, T. S.; Mingo, N. Simulation of Interfacial Phonon Transport in Si−Ge Heterostructures Using an Atomistic Green's Function Method. *J. Heat Transfer* **2006**, *129* (4), 483−491.
(30) Pang, J. W. L.; Buyers, W. J. L.; Chernatynskiy, A.; Lumsden, M. D.; Larson, B. C.; Phillpot, S. R. Phonon Lifetime Investigation of Anharmonicity and Thermal Conductivity of UO_2 by Neutron Scattering and Theory. *Phys. Rev. Lett.* **2013**, *110* (15), 157401.
(31) Giannozzi, P.; Baroni, S.; Bonini, N.; Calandra, M.; Car, R.; Cavazzoni, C.; Ceresoli, D.; Chiarotti, G. L.; Cococcioni, M.; Dabo, I.; et al. Quantum Espresso: A Modular and Open-Source Software Project for Quantum Simulations of Materials. *J. Phys.: Condens. Matter* **2009**, *21* (39), 395502.
(32) Troullier, N.; Martins, J. L. Efficient Pseudopotentials for Plane-Wave Calculations. *Phys. Rev. B* **1991**, *43* (3), 1993−2006.
(33) Yoshizawa, M.; Shirotani, I.; Fujimura, T. Thermal and Elastic Properties of Black Phosphorus. *J. Phys. Soc. Jpn.* **1986**, *55* (4), 1196−1202.
(34) Kôzuki, Y.; Hanayama, Y.; Kimura, M.; Nishitake, T.; Endo, S. Measurement of Ultrasound Velocity in the Single Crystal of Black Phosphorus up to 3.3 GPa Gas Pressure. *J. Phys. Soc. Jpn.* **1991**, *60* (5), 1612−1618.
(35) Cartz, L.; Srinivasa, S. R.; Riedner, R. J.; Jorgensen, J. D.; Worlton, T. G. Effect of Pressure on Bonding in Black Phosphorus. *J. Chem. Phys.* **1979**, *71* (4), 1718−1721.
(36) Cai, Y.; Lan, J.; Zhang, G.; Zhang, Y.-W. Lattice Vibrational Modes and Phonon Thermal Conductivity of Monolayer MoS_2. *Phys. Rev. B* **2014**, *89* (3), 035438.
(37) Xu, Y.; Chen, X.; Gu, B.-L.; Duan, W. Intrinsic Anisotropy of Thermal Conductance in Graphene Nanoribbons. *Appl. Phys. Lett.* **2009**, *95* (23), 233116.
(38) Bae, M.-H.; Ong, Z.-Y.; Estrada, D.; Pop, E. Imaging, Simulation, and Electrostatic Control of Power Dissipation in Graphene Devices. *Nano Lett.* **2010**, *10* (12), 4787−4793.
(39) Estrada, D.; Pop, E. Imaging Dissipation and Hot Spots in Carbon Nanotube Network Transistors. *Appl. Phys. Lett.* **2011**, *98* (7), 073102.
(40) Bae, M.-H.; Islam, S.; Dorgan, V. E.; Pop, E. Scaling of High-Field Transport and Localized Heating in Graphene Transistors. *ACS Nano* **2011**, *5* (10), 7936−7944.
(41) Guo, Z.; Zhang, D.; Gong, X.-G. Thermal Conductivity of Graphene Nanoribbons. *Appl. Phys. Lett.* **2009**, *95* (16), 163103.
(42) Wei, N.; Xu, L.; Wang, H.-Q.; Zheng, J.-C. Strain Engineering of Thermal Conductivity in Graphene Sheets and Nanoribbons: A Demonstration of Magic Flexibility. *Nanotechnology* **2011**, *22* (10), 105705.
(43) Gunawardana, K. G. S. H.; Mullen, K.; Hu, J.; Chen, Y. P.; Ruan, X. Tunable Thermal Transport and Thermal Rectification in Strained Graphene Nanoribbons. *Phys. Rev. B* **2012**, *85* (24), 245417.
(44) Li, X.; Maute, K.; Dunn, M. L.; Yang, R. Strain Effects on the Thermal Conductivity of Nanostructures. *Phys. Rev. B* **2010**, *81* (24), 245318.
(45) Liu, Y.; Xu, F.; Zhang, Z.; Penev, E. S.; Yakobson, B. I. Two-Dimensional Mono-Elemental Semiconductor with Electronically Inactive Defects: The Case of Phosphorus. *Nano Lett.* **2014**, DOI: 10.1021/nl5021393.
(46) Zhang, G.; Zhang, Y.-W. Thermal Conductivity of Silicon Nanowires: From Fundamentals to Phononic Engineering. *Phys. Status Solidi RRL* **2013**, *7* (10), 754−766.